Supplementary Material: Coexistence and tuning of spin-singlet and triplet transport in spin-filter Josephson junctions

Halima Giovanna Ahmad,[1,2,3] Martina Minutillo,[1,3] Roberto Capecelatro,[1] Avradeep Pal,[4,5] Roberta Caruso,[1,6] Gianluca Passarelli,[1,3] Mark Blamire,[4] Francesco Tafuri,[1] Procolo Lucignano,[1,3] and Davide Massarotti[7,3]

[1]*Dipartimento di Fisica E. Pancini, Università degli Studi di Napoli Federico II, Monte S. Angelo, via Cinthia, I-80126 Napoli, Italy*
[2]*Seeqc, Strada Vicinale Cupa Cinthia, 21, I-80126 Napoli, Italy*
[3]*CNR-SPIN, UOS Napoli, Monte S. Angelo, via Cinthia, I-80126 Napoli, Italy*
[4]*Department of Materials Science and Metallurgy, University of Cambridge, 27 Charles Babbage Road, Cambridge CB3 0FS, United Kingdom*
[5]*Department of Metallurgical Engineering and Materials Science, IIT Bombay, Mumbai, 400076, India*
[6]*Brookhaven National Laboratory, Upton, New York 11973-5000, USA*
[7]*Dipartimento di Ingegneria Elettrica e delle Tecnologie dell'Informazione, Università degli Studi di Napoli Federico II, via Claudio, I-80125 Napoli, Italy*

SUPPLEMENTARY NOTE 1. THEORETICAL MODEL

We describe the Superconductor/Ferromagnetic Insulator/Superconductor (S/FI/S) junction using a two-dimensional (2D) lattice model, as shown in Figure 1 of the main text, that we report in Supplementary Figure1.

The Hamiltonian of the junction in the Nambu⊗spin space is given by [1–3]

$$\check{\mathscr{H}} = \sum_{\mathbf{r},\mathbf{r}'} \Psi^{\dagger}(\mathbf{r}) \begin{bmatrix} \hat{H}(\mathbf{r},\mathbf{r}') & \hat{\Delta}(\mathbf{r},\mathbf{r}') \\ -\hat{\Delta}^{*}(\mathbf{r},\mathbf{r}') & -\hat{H}^{*}(\mathbf{r},\mathbf{r}') \end{bmatrix} \Psi(\mathbf{r}'), \tag{1}$$

with $\Psi(\mathbf{r}) = \left[\psi_{\uparrow}(\mathbf{r}), \psi_{\downarrow}(\mathbf{r}), \psi^{\dagger}_{\uparrow}(\mathbf{r}), \psi^{\dagger}_{\downarrow}(\mathbf{r})\right]^{T}$. Here, $\psi^{\dagger}_{\mu}(\mathbf{r})$ and $\psi_{\mu}(\mathbf{r})$ are the field operators creating/destructing an electron with spin μ at the lattice point $\mathbf{r} = j\mathbf{x} + m\mathbf{y}$, with $j = 0, 1, \ldots, L, L+1$ and $m = 1, \ldots, W$.

Here and in the followings, the symbols $\hat{\cdot}$ and $\check{\cdot}$ describe the 2×2 and 4×4 matrices, in spin and Nambu⊗spin spaces respectively.

In Equation 1, $\hat{H}$ is the normal-state Hamiltonian of the junction while $\hat{\Delta}$ describes the superconducting pairing potential. The former can be written as $\hat{H} = \hat{H}_{\mathrm{S}} + \hat{H}_{\mathrm{FI}}$, with $\hat{H}_{\mathrm{S}}$ and $\hat{H}_{\mathrm{FI}}$ referring to the S leads and FI barrier, respectively.

In Supplementary Figure(1), the S regions extend for $j < 1$ and $j > L$. $\hat{H}_{\mathrm{S}}$ consists in a kinetic energy term that reads:

$$\begin{aligned} \hat{H}_{\mathrm{S}}(\mathbf{r},\mathbf{r}') = \big[-t_{\mathrm{s}}\left(\delta_{\mathbf{r},\mathbf{r}'+\mathbf{x}} + \delta_{\mathbf{r}+\mathbf{x},\mathbf{r}'} + \delta_{\mathbf{r},\mathbf{r}'+\mathbf{y}} + \delta_{\mathbf{r}+\mathbf{y},\mathbf{r}'}\right) - \left(4t_{\mathrm{s}} - \mu_{\mathrm{s}}\right)\delta_{\mathbf{r},\mathbf{r}'}\big]\,\hat{\sigma}_0 \\ \times\left[\Theta\left(-j+1\right) + \Theta\left(j-L\right)\right], \end{aligned} \tag{2}$$

where t_{s} and μ_{s} are the hopping parameter and the chemical potential, respectively, and Θ is the Heaviside step-function. Here and in the followings, we indicate with $\hat{\sigma}_0$ and $\hat{\sigma}_\nu$ ($\nu = 1,2,3$) the unit and the Pauli matrices in the spin space, respectively.

In this work, we take the pairing potential Δ different from zero only in the S leads, which, thus, vanishes inside the FI barrier. Here, Δ is of spin singlet s-wave symmetry and is expressed as

$$\hat{\Delta}(\mathbf{r},\mathbf{r}') = \Delta\delta_{\mathbf{r},\mathbf{r}'}\, i\,\hat{\sigma}_2\left[\Theta\left(-j+1\right)\mathrm{e}^{\mathrm{i}\phi_{\mathrm{L}}} + \Theta\left(j-L\right)\mathrm{e}^{\mathrm{i}\phi_{\mathrm{R}}}\right], \tag{3}$$

where $\phi = \phi_{\mathrm{L}} - \phi_{\mathrm{R}}$ is the phase difference across the junction and ϕ_{L} (ϕ_{R}) is the phase in the left (right)-hand side superconductor.

In our model, the order parameter Δ is constant in the leads and it is not derived from self-consistent calculations. Further, we assume that there is no disorder in the superconductors.

The FI extends from $j = 1$ to $j = L$, its normal-state Hamiltonian H_{FI} consists of four terms

$$\hat{H}_{\mathrm{FI}} = \hat{H}_{\mathrm{k}} + \hat{H}_{\mathrm{soc}} + \hat{H}_{\mathrm{ex}} + \hat{H}_{\mathrm{i}}. \tag{4}$$

$\hat{H}_{\mathrm{k}}$ is the kinetic energy,

$$\hat{H}_{\rm k}(\mathbf{r},\mathbf{r}') = \left[-t\left(\delta_{\mathbf{r},\mathbf{r}'+\mathbf{x}} + \delta_{\mathbf{r}+\mathbf{x},\mathbf{r}'} + \delta_{\mathbf{r},\mathbf{r}'+\mathbf{y}} + \delta_{\mathbf{r}+\mathbf{y},\mathbf{r}'}\right) - (4t-\mu_{\rm FI})\,\delta_{\mathbf{r},\mathbf{r}'}\right]\hat{\sigma}_0 \times\Theta(j)\,\Theta(L+1-j)\,. \tag{5}$$

The spin-orbit coupling (SOC) Hamiltonian is

$$\hat{H}_{\rm soc}(\mathbf{r},\mathbf{r}') = i\alpha\left[\left\{\delta_{\mathbf{r},\mathbf{r}'+\mathbf{x}} - \delta_{\mathbf{r}+\mathbf{x},\mathbf{r}'}\right\}\hat{\sigma}_2 - \left\{\delta_{\mathbf{r},\mathbf{r}'+\mathbf{y}} - \delta_{\mathbf{r}+\mathbf{y},\mathbf{r}'}\right\}\hat{\sigma}_1\right]\Theta(j)\,\Theta(L+1-j)\,. \tag{6}$$

The exchange potential is

$$\hat{H}_{\rm ex}(\mathbf{r},\mathbf{r}') = -\mathbf{h}'\cdot\boldsymbol{\sigma}\,\delta_{\mathbf{r},\mathbf{r}'}\Theta(j)\,\Theta(L+1-j)\,, \tag{7}$$

where $\boldsymbol{\sigma}$ is the vector of the Pauli matrices $(\hat{\sigma}_1,\hat{\sigma}_2,\hat{\sigma}_3)$.

The on-site random impurity potential is

$$\hat{H}_{\rm i}(\mathbf{r},\mathbf{r}') = v_{\mathbf{r}}\,\hat{\sigma}_0\,\delta_{\mathbf{r},\mathbf{r}'}\Theta(j)\,\Theta(L+1-j)\quad. \tag{8}$$

Here, we indicate with t the hopping integral among nearest-neighbor lattice sites, $\mu_{\rm FI}$ the Fermi energy, α the amplitude of the spin-orbit interaction, $v_{\mathbf{r}}$ the on-site random impurity potential strength uniformly distributed in the range $-V_{\rm imp}/2 \leq v_{\mathbf{r}} \leq V_{\rm imp}/2$. The exchange field is assumed to be slightly disordered and is modeled as $h' = h + \delta_h$, where δ_h are small on-site fluctuations given randomly in the range $-h/10 \leq \delta_h \leq h/10$ (along the $\mathbf{h}$-direction).

In order to calculate the Josephson current flowing through the junction, we have to evaluate the barrier Green's function (GF) connecting two lattice sites located at $\mathbf{r}$ and $\mathbf{r}'$:

$$\check{G}_{\omega_n}(\mathbf{r},\mathbf{r}') = \begin{bmatrix} \hat{G}_{\omega_n}(\mathbf{r},\mathbf{r}') & \hat{F}_{\omega_n}(\mathbf{r},\mathbf{r}') \\ -\hat{F}^*_{\omega_n}(\mathbf{r},\mathbf{r}') & -\hat{G}^*_{\omega_n}(\mathbf{r},\mathbf{r}') \end{bmatrix}, \tag{9}$$

where, as before, $\hat{G}$ and $\check{G}$ are matrices in the spin and Nambu$\otimes$spin space respectively. $\check{G}$ solves the following Gor'kov equation [1–3]

$$\left[i\omega_n\hat{\tau}_0\hat{\sigma}_0 - \sum_{\mathbf{r}_1}\begin{pmatrix} \hat{H}(\mathbf{r},\mathbf{r}_1) & \hat{\Delta}(\mathbf{r},\mathbf{r}_1) \\ -\hat{\Delta}^*(\mathbf{r},\mathbf{r}_1) & -\hat{H}^*(\mathbf{r},\mathbf{r}_1)\end{pmatrix}\right]\times\check{G}_{\omega_n}(\mathbf{r}_1,\mathbf{r}') = \hat{\tau}_0\hat{\sigma}_0\delta(\mathbf{r}-\mathbf{r}'), \tag{10}$$

where $\omega_n = (2n+1)\pi T$ is the fermionic Matsubara frequency and T is a temperature. Here and in the followings, we indicate with $\hat{\tau}_0$ and $\hat{\tau}_\nu$ ($\nu = 1,2,3$) the analogous of the unit and Pauli matrices in the Nambu space, respectively.

In this work, we use the Recursive Green's Function (RGF) technique [1–3] to solve the Gor'kov Equation 10 and obtain the Josephson current from the GFs connecting two adjacent sites along the $\mathbf{x}$-direction (namely $\check{G}_{\omega_n}(\mathbf{r},\mathbf{r}+\mathbf{x})$ and $\check{G}_{\omega_n}(\mathbf{r}+\mathbf{x},\mathbf{r})$), that we can write as

$$J = -\frac{\mathrm{i}\,\mathrm{e}}{2}T\sum_{\omega_n}\sum_{m=1}^{W} Tr\left[\hat{\tau}_3\check{T}_+\check{G}_{\omega_n}(\mathbf{r},\mathbf{r}+\mathbf{x}) - \hat{\tau}_3\check{T}_-\check{G}_{\omega_n}(\mathbf{r}+\mathbf{x},\mathbf{r})\right], \tag{11}$$

where Tr stands for the trace over the Nambu$\otimes$spin space. Here, $\check{T}_\pm$ matrices describe the hopping and the SOC along the propagation direction ($\mathbf{x}$-direction) [3], and read:

$$\check{T}_\pm = \begin{pmatrix} -t\hat{\sigma}_0 \mp i\alpha\hat{\sigma}_2 & 0 \\ 0 & t\hat{\sigma}_0 \pm i\alpha\hat{\sigma}_2\end{pmatrix}. \tag{12}$$

In Equation 11, in order to consider the contribution of all the lattice sites along the **y**-direction, the summation $\sum_{m=1}^{W}$ is performed. Furthermore, the summation over the Matsubara frequencies is made until the convergence condition is reached. Then, we calculate the current-phase relation (CPR) from Equation 11 at fixed temperature T by varying the phase difference ϕ between the S leads from 0 to π. Finally, we compute the $I_c(T)$ curves from the maximum of the CPRs at temperature T ranging from 0 to the critical temperature T_c.

The off-diagonal terms of the matrix in the right-hand side of Equation 9 are the so-called anomalous Green's functions $\hat{F}_{\omega_n}$. From these latter, taking the elements with $\mathbf{r}' = \mathbf{r} = j\mathbf{x} + m\mathbf{y}$, we can derive the four pairing components with s-wave symmetry at each position j along the **x**-direction [3]:

$$\frac{1}{W}\sum_{\omega_n}\sum_{m=1}^{W}\hat{F}_{\omega_n}(\mathbf{r},\mathbf{r}) = \sum_{\nu=0}^{3} f_\nu \hat{\sigma}_\nu \, i\,\hat{\sigma}_2 \,, \tag{13}$$

where f_0 is the spin singlet component and f_ν with $\nu = 1,2,3$ are the spin-triplet components. Here, similarly to Equation 11, the summation $\sum_{m=1}^{W}$ is performed to take into account all the lattice sites with the same longitudinal coordinate j and different index m in the transverse direction.

Analogous considerations can be applied to the GFs connecting the sites at the position $\mathbf{r}$ with their neighbors in $\mathbf{r}-\mathbf{x}$ and $\mathbf{r}+\mathbf{x}$, from which we can calculate the odd-parity p-wave pairing functions. Thus, the p-wave correlations inside the barrier, at the position j along **x**-direction ($\mathbf{r} = j\mathbf{x} + m\mathbf{y}$), can be expressed as:

$$\frac{1}{4W}\sum_{\omega_n}\sum_{m=1}^{W}\left[\hat{F}_{\omega_n}(\mathbf{r}+\mathbf{x},\mathbf{r}) + \hat{F}_{\omega_n}(\mathbf{r},\mathbf{r}-\mathbf{x}) - \hat{F}_{\omega_n}(\mathbf{r},\mathbf{r}+\mathbf{x}) - \hat{F}_{\omega_n}(\mathbf{r}-\mathbf{x},\mathbf{r})\right] = \tag{14}$$

$$\sum_{\nu=0}^{3} f_\nu \hat{\sigma}_\nu \, i\,\hat{\sigma}_2.$$

Making explicit the second term in Equation 13 (Equation 14), we can rewrite the s-wave (p-wave) pairing components as

$$\begin{cases} f_0 = \dfrac{f_{\uparrow\downarrow} - f_{\downarrow\uparrow}}{2} \\ f_3 = \dfrac{f_{\uparrow\downarrow} + f_{\downarrow\uparrow}}{2} \\ f_1 = \dfrac{f_{\downarrow\downarrow} - f_{\uparrow\uparrow}}{2} \\ f_2 = \dfrac{f_{\uparrow\uparrow} + f_{\downarrow\downarrow}}{2i}, \end{cases} \tag{15}$$

from which we extract the standard spin correlation functions, f_0, f_3, $f_\uparrow$ (that is $f_{\uparrow\uparrow}$) and $f_\downarrow$ (that is $f_{\downarrow\downarrow}$).

SUPPLEMENTARY NOTE 2. SIMULATION PARAMETERS

In the following, we report the choice of the model parameters used in the paper. Henceforth, we adopt units with $\hbar = c = k_B = 1$, where c is the speed of light, k_B is the Boltzmann constant and $\hbar$ is the reduced Planck constant.

The junction plane coincides with the xy-plane whereas the exchange field $\mathbf{h}'$ is always in the perpendicular direction $\mathbf{h}' = h'\mathbf{z}$ (along the **z**-direction).

All the energy parameters are expressed in dimensionless units where the energy scale is the hopping t in the FI. The α is scaled by ta (with a lattice constant), while the Josephson current is calculated in units of $J_0 = e\Delta$.

In our simulations, we fix several parameters as $t = 1$, $\mu_{FI} = 0$, $\mu_s = 3$, $\Delta = 0.005$, $h = 0.25$. Further, we note that NbN (S leads) and GdN (FI barrier) are characterized by almost equal hopping parameters [4–6], which are, thus, set equal $t_s = t$ for the sake of simplicity. As a matter of fact, in order to have a good agreement with experimental data, we model these devices as tunnel junctions with GdN barrier in the ferromagnetic half metal regime [7–9]. Thus, we choose to assume different chemical potentials for the S and FI regions. The estimate for the exchange energy $h = |\mathbf{h}|$ is chosen in agreement to the exchange field

measured in several works for the bulk GdN [5, 6, 10–12], given that $t \approx 3\,\text{eV}$ [4–6] and the experimental constant lattice of GdN is $a_{\text{GdN}} = 4.974\,\text{Å}$.

When modeling the experiments, we use α as a measure of the spin-mixing and it is chosen to be $\alpha = 0.04$, unless otherwise indicated. Although we choose a small spin-orbit field so that $\alpha \ll h$, it breaks the spin symmetry at interfaces and is sufficient to cause the generation of long-range equal-spin triplet correlations with total spin projection $S_z = \pm 1$.

Finally, we take V_{imp} in the range $0.05 - 0.50$. The chosen values of V_{imp} will be reported below where we will specify our considerations to the different analyses carried out in the main text. Due to the presence of disorder, we perform ensemble averages over several samples to obtain the final $I_c(T)$ curves and correlations. In particular, we use $N_S = 50 - 100$ samples to compute the average $I_c(T)$ and $N_S = 200 - 300$ samples for the average correlation functions, depending on the strength of V_{imp}.

For the $I_c(T)$ curves in Figure(2) in the main text (as for the corresponding correlation functions in Figure(3)), we choose systems with dimensions in the **x** and **y** directions, respectively: (a) $L = 8$, $W = 24$, (b) $L = 8$, $W = 28$, (c) $L = 8, W = 32$, expressed in units of lattice sites.

Tunnel junctions experience an exponential suppression of the critical current when increasing the barrier thickness. In our model, this implies dealing with systems of few lattice sites, hence, we choose $L = 8$ and keep it fixed in all the numerical simulations, in agreement with the short-junction limit.

However, the main effect of increasing the experimental sample thickness (and so the magnetic area of the FI) consists in enhancing the magnetic activity of the junction [13].

In our model, we manage to mimic this effect by changing the flux of the exchange field $\Phi(h) = LWh$ through the JJ (by the means of the width of the barrier W) and by tuning the impurity potential strength V_{imp} (thus, changing the influence of disorder effects in the system).

In particular, by varying the width of the barrier W, we change the JJ effective area. In this way, we are able to control the exchange field flux $\Phi(h) = LWh$, without modifying the value of h, which is kept fixed to that of the bulk GdN [5, 6, 10–12].

In Figure(2), we set $V_{\text{imp}} = 0.3$ for the simulation in (a), $V_{\text{imp}} = 0.37$ in (b), and $V_{\text{imp}} = 0.23$ in (c), thus, tuning the disorder effects in each simulated device.

Therefore, we use $\Phi(h)$ and V_{imp} as effective control parameters to model the peculiar $I_c(T)$ behavior of different junctions.

We notice that the Hamiltonian parameters, as well as the lattice size, have no microscopic origin and are chosen to describe the main mechanisms that are expected to occur in the experimental devices. Even though the lattice size is scaled down compared to the experimental system, we think that our theoretical model should give qualitatively an accordance with the experimental results as long as the model parameters are adjusted accordingly.

In Figure(5) in the main text, we consider the $L = 8, W = 32$ junction. Here, we take different impurity potential values for each computed $I_c(T)$ curve (along with the corresponding spin-correlation functions); $V_{\text{imp}} = 0.3$, $V_{\text{imp}} = 0.23$ and $V_{\text{imp}} = 0.05$.

To investigate on the role of spin-orbit coupling and impurities in a more general framework, in Figure(6) the $L = 8, W = 32$ junction is also analyzed for different values of SOC and of impurity potential (α and V_{imp}, respectively). To accomplish the $I_c(T)$ diagram, we select the following values for the α and V_{imp} - axes: $\alpha = 0.04, 0.07, 0.1, 0.2$ and $V_{\text{imp}} = 0.05, 0.23, 0.3, 0.5$.

SUPPLEMENTARY FIGURE 1

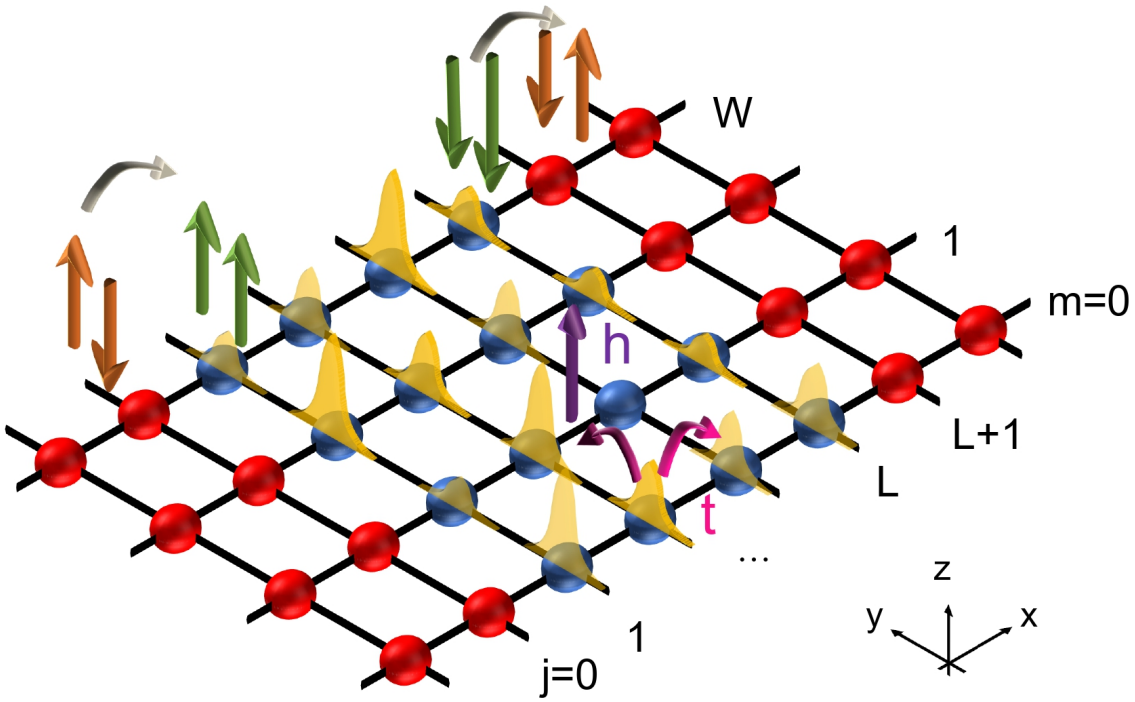

Supplementary Figure 1: **Two-dimensional lattice model scheme**. Picture of the Superconductor/Ferromagnetic Insulator/Superconductor two-dimensional lattice model. The barrier (blue sites) has a total thickness L along **x** and the junction width is W along **y**. The spin-rotation mechanism due to the spin-orbit coupling is depicted by the spin-flipping process highlighted at the interface between the superconducting boundaries (red sites) and the barrier. The impurities, with random strength depicted by the height of the yellow potential peak, are represented on each site of the lattice. The exchange field h is parallel to the **z** axis, while the hopping t between nearest-neighbour sites is here represented by pink arrows.

SUPPLEMENTARY FIGURE 2

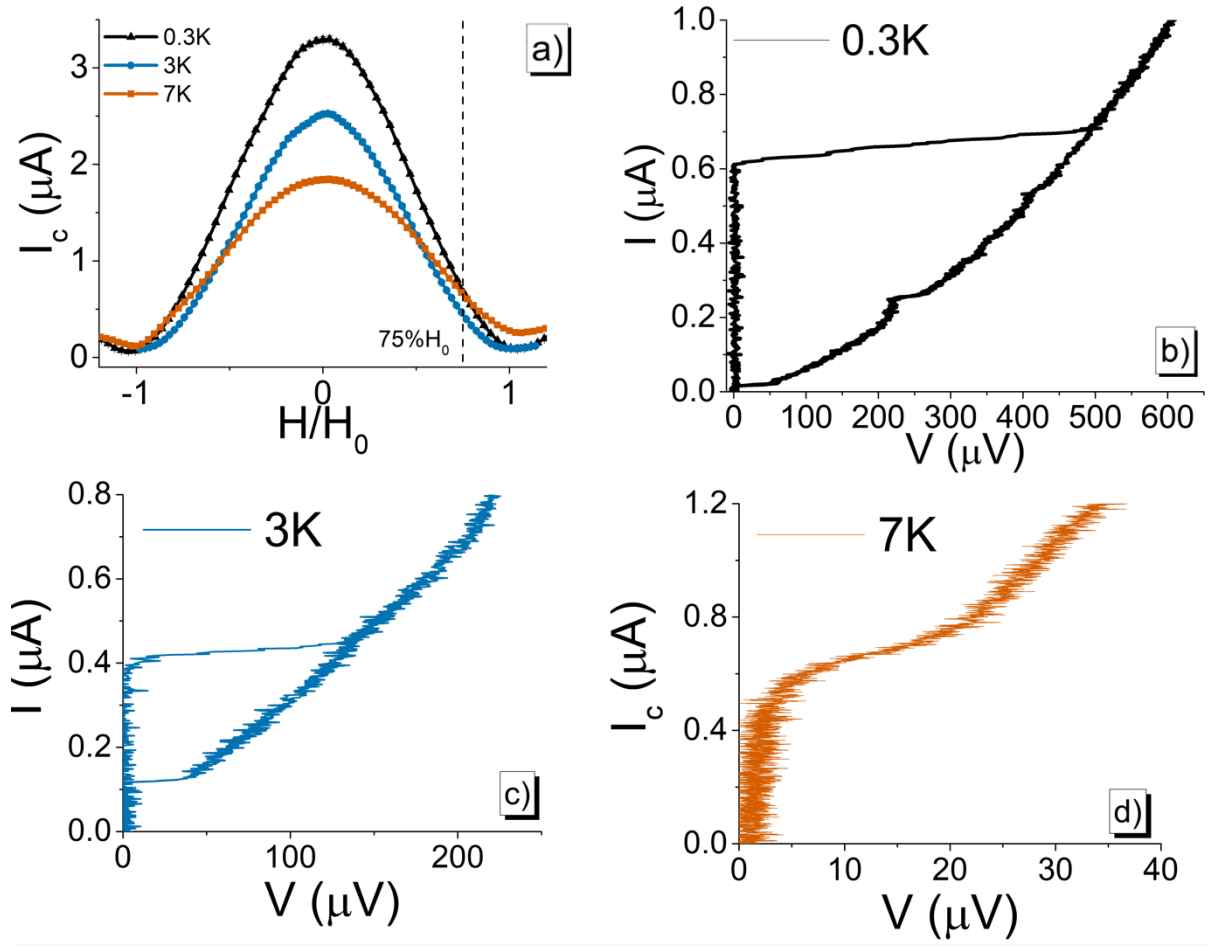

Supplementary Figure 2: **Fraunhofer pattern curves.** In (a), Fraunhofer pattern curves measured at 0.3 K (black triangles), at 3 K (blue circles) and at 7 K (red squares) for the Josephson junction with $d_F = 3.0$ nm. Straight lines are only a guide for the eye. The magnetic field H is normalized to the magnetic field periodicity H_0. As shown in Figure 4 (b) of the main manuscript, 3 K and 7 K correspond to minimum and maximum, respectively, of the critical current vs. temperature $I_c(T)$ curve for a magnetic field $H/H_0 = 75\%$. The shift of the Fraunhofer pattern curve due to the magnetic hysteresis of the barrier has been removed in post-processing in order to ensure the comparison between the different Fraunhofer curves. The dashed line in (a) refers to the magnetic field corresponding to $75\%H_0$. The $I(V)$ curves measured at $H = 75\%H_0$ at the same temperatures reported in (a) are reported as a reference: (b) at 0.3 K, (c) at 3 K and (d) at 7 K.

SUPPLEMENTARY FIGURE 3

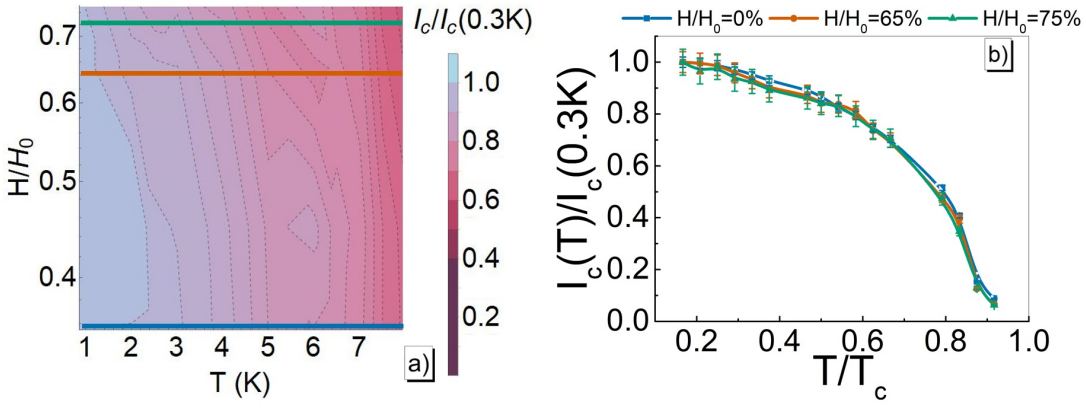

Supplementary Figure 3: **Tuning of the temperature dependence of the critical current in presence of an external magnetic field for a non spin-filter Josephson junction.** In (a), normalized critical current $I_c(T, H/H_0)/I_c(0.3\,\mathrm{K}, H/H_0)$ density plot as a function of the percentage of periodicity H/H_0 and the temperature T, for a non spin-filter Josephson junction with GdN thickness $d_F = 1.5\,\mathrm{nm}$. Straight lines in (a) refer to the cross sections reported in (b): blue and square symbols for $H/H_0 = 0\%$, red and circle symbols for $H/H_0 = 65\%$ and green and triangle symbols for $H/H_0 = 75\%$. In non spin-filter Josephson junctions the Ambegaokar-Baratoff [14] trend is preserved for any applied magnetic field, indicating the important role of the magnetic activity in the system.

SUPPLEMENTARY REFERENCES

[1] A. Furusaki, Dc josephson effect in dirty SNS junctions: Numerical study, Physica B: Condensed Matter **203**, 214 (1994).
[2] Y. Asano, Numerical method for dc Josephson current between d-wave superconductors, Phys. Rev. B **63**, 052512 (2001).
[3] T. Yamashita, J. Lee, T. Habe, and Y. Asano, Proximity effect in a ferromagnetic semiconductor with spin-orbit interactions, Phys. Rev. B **100**, 094501 (2019).
[4] L. Litinskii, The band structure of hexagonal nbn, Solid state communications **71**, 299 (1989).
[5] F. Leuenberger, W. Parge, A.and Felsch, K. Fauth, and M. Hessler, GdN thin films: Bulk and local electronic and magnetic properties, Physical Review Letters B 72, 014427 (2005).
[6] L. E. Marsoner Steinkasserer, B. Paulus, and N. Gaston, Hybrid density functional calculations of the surface electronic structure of GdN, Phys. Rev. B **91**, 235148 (2015).
[7] C.-g. Duan, R. F. Sabiryanov, J. Liu, W. N. Mei, P. A. Dowben, and J. R. Hardy, Strain induced half-metal to semiconductor transition in GdN, Phys. Rev. Lett. **94**, 237201 (2005).
[8] P. Larson and W. R. L. Lambrecht, Electronic structure of Gd pnictides calculated within the $LSDA + U$ approach, Phys. Rev. B **74**, 085108 (2006).
[9] P. Wachter and E. Kaldis, Magnetic interaction and carrier concentration in GdN and $GdN_{1-x}O_x$, Solid State Communications **34**, 241 (1980).
[10] A. Pal and M. G. Blamire, Large interfacial exchange fields in a thick superconducting film coupled to a spin-filter tunnel barrier, Phys. Rev. B **92**, 180510 (2015).
[11] J. P. Cascales, Y. Takamura, G. M. Stephen, D. Heiman, F. S. Bergeret, and J. S. Moodera, Switchable Josephson junction based on interfacial exchange field, Applied Physics Letters **114**, 022601 (2019), https://doi.org/10.1063/1.5050382.
[12] A. Manchon, H. C. Koo, J. Nitta, S. M. Frolov, and R. A. Duine, New perspectives for Rashba spin–orbit coupling, Nature Materials **14**, 871–882 (2015).
[13] R. Caruso, D. Massarotti, G. Campagnano, A. Pal, H. G. Ahmad, P. Lucignano, M. Eschrig, M. G. Blamire, and F. Tafuri, Tuning of magnetic activity in spin-filter Josephson junctions towards spin-triplet transport, Phys. Rev. Lett. **122**, 047002 (2019).
[14] V. Ambegaokar and A. Baratoff, Tunneling between superconductors, Phys. Rev. Lett. **10**, 486 (1963).